Crystal Structure of 2-Amino-5-Nitropyridinium Dihydrogenphosphate Monophosphoric Acid: Influence of the Polyanion Charge on the Formation of Centrosymmetric Structure

Julien Zaccaro, Muriel Bagieu-Beucher,[1] Alain Ibanez, and René Masse

C.N.R.S., Laboratoire de Cristallographie, associé à l'Université J. Fourier, B.P. 166, 38042 Grenoble Cédex 09, France

Chemical preparation and structural characterization by single crystal X-ray diffraction are given for the 2-amino-5-nitropyridinium dihydrogenphosphate monophosphoric acid (2A5NPDPP): $C_5H_6N_3O_2^+ \cdot H_2PO_4^- \cdot H_3PO_4$. Crystals are monoclinic, space group $P\,2_1/n$ with $a = 16.050(16)$, $b = 8.985(5)$, $c = 8.830(5)$ Å, $\beta = 96.86(7)°$, $V = 1264(2)$ Å^3, $Z = 4$. The structure was refined to $R = 0.050$ ($R_W = 0.056$) for 2224 reflections with $I \geq 3\sigma(I)$. The structural arrangement can be described as inorganic layers of $H_5P_2O_8^-$ units separated by infinite organic chains of chromophores. Strong hydrogen bonds maintain a two-dimensional cohesion between phosphate tetrahedra while weaker ones link the organic cations together and to the anionic subnetwork. The influence of the polyanion charge on the symmetry of the cationic packing is discussed with respect to the herringbone structure of the 2-amino-5-nitropyridinium dihydrogenphosphate (2A5NPDP), a nonlinear optical crystal built with the same chromophores. © 1996 Academic Press, Inc.

INTRODUCTION

A new class of noncentrosymmetric crystals for quadratic nonlinear optics has recently been developed through a crystal engineering route which combines the high cohesion of inorganic host-matrices with the enhanced polarizability of organic guest-chromophores (1). Several noncentrosymmetric phases including the 2-amino-5-nitropyridinium cations as nonlinear optical (NLO) entities have been prepared (2, 3). The cations are anchored onto the host-matrices through hydrogen bonds, inducing a higher packing cohesion than that observed in NLO organic crystals. The herringbone motif of cations in such noncentrosymmetric structures depends upon the ability of host anions to aggregate. A correlation between the minimum intercation distance measured on both sides of

the anionic matrix and the noncentrosymmetry of the framework has been observed: this has made it possible to engineer new noncentrosymmetric structures in selecting appropriate anionic aggregates (4, 5). If in this case the aggregation ability of anions is a factor which influences the building of herringbone structures, a second factor to take into account could be the charge associated with the volume of anions (monomer). We had used this assumption to explain the formation of centrosymmetric structures of 2-amino-5-nitropyridinium nitrate and tetrachlorocuprate (6) with respect to the herringbone structure of 2-amino-5-nitropyridinium dihydrogenphosphate (2A5NPDP) (2). The crystal structure of 2-amino-5-nitropyridinium dihydrogenphosphate monophosphoric acid (2A5NPDPP) has been investigated to emphasize the role played by the $H_5P_2O_8^-$ monomer in the organization of centrosymmetric packing in contrast to that played by $H_2PO_4^-$ in the formation of the 2A5NPDP herringbone structure.

EXPERIMENTAL

Crystal Synthesis

Crystals of 2A5NPDPP were accidentally grown in H_3PO_4-rich solutions used for the synthesis of large amounts of 2A5NPDP, a step very useful for growing large single crystals of this NLO material. After several crystallizations by evaporation of 2A5NPDP from H_3PO_4 (2–4 M) initial solutions, the molarity of the phosphoric solutions increases and provides, for high H_3PO_4 concentrations (up to 10 M, pH < 0), white single crystals. The chemical formula of this new material, 2-amino-5-nitropyridinium dihydrogenphosphate monophosphoric acid (2A5NPDPP), was determined by X-ray crystal structure analysis. These crystals decompose slowly due to air moisture, as further explained by the observation of weak hydrogen bonds between the cation–anion subnetworks in the crystal structure and by the strong Brønsted basicity of the $H_5P_2O_8^-$

TABLE 1
Lattice Parameters of $C_5H_6N_3O_2^+ \cdot H_5P_{2-x}As_xO_8^-$ Solid Solutions

ρ^a in solution (mole %)	ρ in crystalline sample[b]	**a** (Å)	**b**	**c**	$\beta(°)$
0	0	16.07(1)	8.993(6)	8.831(4)	96.82(3)
45	40.7	16.09(1)	8.997(9)	8.850(9)	96.79(5)
60	56.0	16.09(1)	8.995(6)	8.860(5)	96.70(5)
80	74.8	16.09(1)2	8.99(1)	8.865(9)	96.81(6)
90	85.4	16.110(8)	9.004(6)	8.865(5)	96.79(4)
100	100	16.10(1)	8.994(8)	8.892(9)	96.76(3)

[a] ρ is the molar percentage of $H_5P_2O_8^-$.

[b] ρ determined by scanning electron microscopy, averaged on two samples.

Note. Cell parameters have been refined by a least-squares method using data from X-ray powder diffractograms collected at $\lambda_{CuK\alpha}$.

TABLE 2
Crystal Data, Intensity Measurements and Structural Refinement Parameters

Formula	$C_5H_6N_3O_2^+ \cdot H_2PO_4^- \cdot H_3PO_4$
Molecular weight	335.11
Space group	$P2_1/n$
a (Å)	16.050(16)
b	8.985(5)
c	8.830(5)
$\beta(°)$	96.86(7)
V (Å³)	1264(2)
Z, D_x (g cm⁻³)	4, 1.760
Unit-cell refinement	24 reflect ($10 < \theta < 12°$)
$F(000)$	688
μ (mm⁻¹)	0.219 ($\lambda_{AgK\alpha}$)
Crystal size (mm)	$0.9 \times 0.9 \times 0.9$
Temperature (K)	293
Apparatus	Nonius CAD4
Monochromator	graphite (220)
Radiation (Å)	0.5608 (Ag $K\alpha$)
Bragg angle limits (°)	3–25
Scan technique	ω scan
Back ground(sec)	5–20
Scan speed (° sec⁻¹)	0.03 to 0.11
Scan width (°)	1.20
Control reflections:	
Intensity every	7200 sec (no decay)
Orientation every	400 reflections
Reflections collected	2426
Unique data	2270 ($R_{int} = 0.030$)
Data used in refinement	2224 ($I > 3\sigma(I)$)
Refined parameters	225
R (R_w)	0.050 (0.056)
Weighting scheme	unitary
Goodness of fit	1.271
Largest shift/error	0.03
Max. residual density (e Å⁻³)	0.69
Min. residual density (e Å⁻³)	0.42
Crystallographic system	SDP (9)

anion. Good crystallization conditions of the 2A5NPDPP phase are obtained in H_3PO_4 (12–14 M) solutions either from the 2A5NPDP salt using a 2A5NPDP/H_3PO_4 molar ratio of around 1/4 or from the 2A5NP molecular compound in the same molar ratio. In such acidic concentrations, the $H_5P_2O_8^-$ anion is the prevailing species in solution (7), explaining the preferential crystallization of 2A5NPDPP ($C_5H_6N_3O_2^+ \cdot H_5P_2O_8^-$).

2A5NPDPP–2A5NPDAsAs Solid Solution

A continuous solid solution, $C_5H_6N_3O_2^+ \cdot H_5P_{2-x}As_xO_8^-$, has been evidenced by X-ray powder diffraction in the full ($0 \leq x \leq 1$) pseudobinary range 2A5NPDPP–
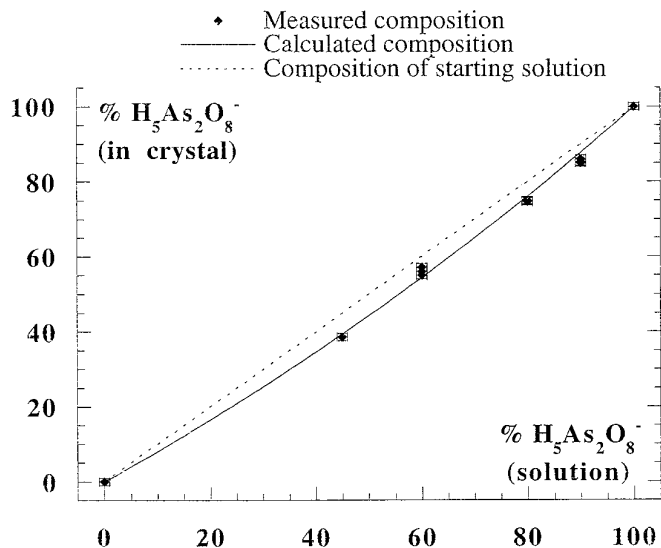

FIG. 1. Composition shift in % between crystal and mother solution in $C_5H_6N_3O_2^+ \cdot H_5P_{2-x}As_xO_8^-$ solid solutions.

2A5NPDAsAs (2-amino-5-nitropyridinium dihydrogen-arsenate monoarsenic acid). The crystal synthesis is similar to that of 2A5NPDPP salt but uses various ratios of H_3PO_4 and H_3AsO_4 acids. The chemical analysis of crystals by electron microscopy (energy dispersive X-ray analysis) revealed a significant deviation from the composition of the starting solutions (Table 1). This shift is well explained by the difference between the ionic dissociation of H_3PO_4 and H_3AsO_4 aqueous solutions. Indeed, the molar ratio of $H_5As_2O_8^-$ anions in H_3PO_4/H_3AsO_4 mixed solutions to all the $H_5X_2O_8^-$ anions (X = P and As), can be expressed as

$$\rho(H_5As_2O_8^-) = \frac{K_a(As)/K_a(P)}{1/\rho(H_3AsO_4) + (K_a(As)/K_a(P) - 1)/100}$$

[1]

where $\rho(H_3AsO_4)$ is the molar percentage of arsenic acid

TABLE 3
Final Atomic Coordinates, Equivalent Temperature Factors B_{eq} (Å^2) for Nonhydrogen Atoms, and Isotropic B_{iso} (Å^2) for Hydrogen Atoms

Atom	x	y	z	B_{eq}/B_{iso}^*
P1	0.87526(5)	0.4854(1)	0.3980(1)	2.10(1)
P2	0.39791(5)	0.4880(1)	0.8207(1)	2.23(2)
O1	0.7873(1)	0.5292(4)	0.4368(3)	3.07(6)
O2	0.8679(2)	0.3964(3)	0.2470(4)	3.20(6)
O3	0.9071(2)	0.3801(3)	0.5326(3)	2.86(5)
O4	0.9237(2)	0.6153(3)	0.3836(4)	3.03(6)
O5	0.3864(2)	0.5115(4)	0.9902(3)	3.68(7)
O6	0.3787(2)	0.6381(4)	0.7354(4)	3.64(7)
O7	0.4858(2)	0.4356(4)	0.8066(3)	3.04(6)
O8	0.3303(2)	0.3808(3)	0.7522(4)	2.97(6)
O9	0.8114(2)	0.2657(4)	0.9007(5)	4.63(8)
O10	0.9439(2)	0.2763(4)	0.8773(5)	4.47(8)
N1	0.8757(2)	0.3355(4)	0.8881(4)	3.16(7)
N2	0.8602(3)	0.9486(4)	0.8690(5)	4.25(9)
N3	0.9271(2)	0.7268(4)	0.8304(4)	2.74(6)
C1	0.8706(2)	0.4960(4)	0.8857(4)	2.28(6)
C2	0.9334(2)	0.5773(5)	0.8374(5)	2.64(7)
C3	0.7950(3)	0.7175(5)	0.9256(5)	3.13(8)
C4	0.8606(3)	0.8020(5)	0.8757(5)	2.77(7)
C5	0.7988(2)	0.5670(5)	0.9305(5)	2.81(8)
H1	0.761(3)	0.570(6)	0.380(6)	2(1)*
H2	0.859(3)	0.313(5)	0.242(5)	1(1)*
H3	0.950(4)	0.368(8)	0.544(7)	5(2)*
H4	0.414(3)	0.554(5)	1.029(5)	1(1)*
H5	0.400(3)	0.714(5)	0.777(5)	1(1)*
H6	0.887(3)	0.991(6)	0.840(5)	1(1)*
H7	0.827(4)	1.008(7)	0.915(7)	4(1)*
H8	0.960(3)	0.769(6)	0.792(6)	3(1)*
H9	0.983(3)	0.537(6)	0.801(6)	2(1)*
H10	0.755(3)	0.759(6)	0.958(6)	2(1)*
H11	0.757(3)	0.506(5)	0.972(5)	1(1)*

Note. The estimated standard deviations are given in parentheses. $B_{eq} = \frac{4}{3}\sum_i \sum_j \mathbf{a}_j \cdot \mathbf{b}_j \cdot \beta_{ij}$.

in the starting solution with respect to the initial molarity of the whole H_3XO_4 (X = P and As).

The relation [1], based on the acid dissociation constants of H_3PO_4 ($K_a(P)$) and H_3AsO_4 ($K_a(As)$), assumes that all the H_3XO_4 molecules and the $H_2XO_4^-$ anions form dimers at 12–14 M acidic concentrations. This assumption is justified by previous work (7) which demonstrated that highly concentrated H_3XO_4 acid solutions are composed mainly of a high content of $H_5X_2O_8^-$ anions and a lower one of $H_6X_2O_8$ molecules. This leads to good agreement between the measured values of $\rho(H_5As_2O_8^-)$ in the crystals and those calculated from Eq. [1] in the corresponding solutions (Fig. 1).

Crystal compositions being accurately known, the cell parameters (Table 1) were refined from the X-ray powder diffraction patterns by a least-squares method on the basis of the 2A5NPDPP crystal structure. The linear composi-

TABLE 4
Main Interatomic Distances (Å) and Bond Angles (°) with e.s.d.'s in Parentheses

The PO_4 Tetrahedron in the H_3PO_4 Molecule

P1	O1	O2	O3	O4
O1	1.543(3)	2.534(4)	2.411(4)	2.555(4)
O2	110.2(2)	1.547(3)	2.529(4)	2.472(4)
O3	102.2(2)	109.2(2)	1.556(3)	2.549(4)
O4	114.1(2)	108.2(2)	112.8(2)	1.503(3)

P1–O1–H1 116(4)
P1–O2–H2 124(4)
P1–O3–H3 116(5)

The PO_4 Tetrahedron in the $H_2PO_4^-$ Anion

P2	O5	O6	O7	O8
O5	1.544(3)	2.511(5)	2.502(4)	2.481(4)
O6	108.1(2)	1.557(3)	2.530(4)	2.449(4)
O7	110.2(2)	111.3(2)	1.506(3)	2.533(4)
O8	108.0(2)	105.4(2)	113.6(2)	1.522(3)

P2–O5–H4 115(4)
P2–O6–H5 117(3)

P1–P1 4.198(1)   P1–P2 4.330(1)
P2–P2 4.281(1)   P1–P2 4.581(1)

The 2-Amino-5-Nitropyridinium Cation

N2–C4	1.319(6)	H6–N2–H7	107(6)
N3–C2	1.348(6)	C2–N3–C4	122,6(4)
N3–C4	1.362(6)	C2–N3–H8	118(4)
N3–H8	0.76(6)	C4–N3–H8	120(4)
C1–C2	1.354(5)	C2–C1–C5	120.5(4)
C1–C5	1.415(5)	C2–C1–N1	120.1(4)
C2–H9	0.96(5)	C5–C1–N1	119.5(4)
C3–C4	1.412(6)	C1–N1–O9	117.8(4)
C3–C5	1.354(7)	C1–N1–O10	118.6(4)
C3–H10	0.82(5)	O9–N1–O10	123.6(4)
C3–H11	0.96(5)	N3–C2–C1	119.8(4)
C1–N1	1.445(5)	N3–C2–H9	115(3)
N1–O9	1.223(5)	C1–C2–H9	125(3)
N1–O10	1.231(5)	C4–C3–C5	120.9(4)
		C4–C3–H10	120(4)
		C5–C3–H10	119(4)
		N2–C4–N3	118.9(4)
		N2–C4–C3	123.4(4)
		N3–C4–C3	117.7(4)

Equation of Least-Squares Plane of Pyridinium Ring and Shifts of Atoms from it (Å)

$5.51(3)x + 0.46(1)y + 7.86(4)z + 11.98(2) = 0$ (crystallographic equation)

Atoms Used in Finding the Least-Squares Plane Equation

N3 0.015(4)	C1 −0.004(4)	C2 −0.008(4)
C3 −0.002(5)	C4 −0.010(4)	C5 0.008(4)

Atoms of Functional Groups

O9 0.310(4)	O10 −0.241(4)	N1 0.023(4)
N2 −0.022(5)	H6 0.04(5)	H7 −0.23(6)

TABLE 5
Hydrogen Bond Schemes in the 2A5NPDPP and
2A5NPDP Structures

D—H⋯A	D–H (Å)	H⋯A (Å)	D⋯A(Å)	D–H⋯A (°)
Hydrogen bonds in $C_5H_6N_3O_2^+ \cdot H_2PO_4^- \cdot H_3PO_4$ (2A5NPDPP)				
O1—H1⋯O8	0.71(5)	1.82(5)	2.500(4)	159(6)
O2—H2⋯O8	0.77(5)	1.80(5)	2.564(4)	172(5)
O3—H3⋯O4	0.69(6)	1.92(6)	2.590(3)	163(7)
O5—H4⋯O7	0.66(5)	2.03(4)	2.603(4)	146(5)
O6—H5⋯O4	0.83(5)	1.84(5)	2.665(4)	172(5)
N2—H7⋯O1	0.89(6)	2.39(6)	3.169(6)	148(5)
N2—H7⋯O9	0.89(6)	2.33(6)	2.976(5)	130(5)
N3—H8⋯O7	0.76(6)	1.98(6)	2.710(5)	159(6)
C2—H9⋯O2	0.96(5)	2.55(5)	3.369(5)	143(4)
C5—H11⋯O5	0.96(5)	2.38(4)	3.212(5)	145(4)
Hydrogen bonds in $C_5H_6N_3O_2^+ \cdot H_2PO_4^-$ (2A5NPDP) (Ref. (2))				
O2—H(O2)⋯O1	0.52(3)	2.21(3)	2.728(2)	169(5)
O3—H(O3)⋯O1	0.72(3)	1.82(3)	2.531(2)	174(3)
N1—H1(N1)⋯O4	0.81(3)	2.04(3)	2.839(2)	165(3)
N1—H2(N1)⋯O1	0.84(2)	2.02(2)	2.862(2)	173(2)
N3—H(N3)⋯O4	0.77(3)	1.89(3)	2.641(2)	166(3)

tion dependence of these parameters shows that the Vegard's law is verified.

2A5NPDPP Crystal Structure Investigation

Cell parameters, space group, and crystal structure were determined from single crystal X-ray diffraction data obtained with a four-circle diffractometer. Crystal data, experimental conditions used during the measurements, and structural refinement parameters are given in Table 2. The crystal selected for the data collection was sealed in a capillary immersed in the growing solution. Because of such conditions and the polyhedral form of the sample no absorption correction was applied, only Lorentz and polarization effects were taken into account. The structure was solved by direct method using MULTAN 77 (8). Full-matrix least-squares refinements were performed on F, the function minimized being $\Sigma w |F_o - |Fc||$ with a unitary weighting scheme. Scattering factors for neutral atoms and f', $\Delta f'$, f'', $\Delta f''$ were taken from the International Tables
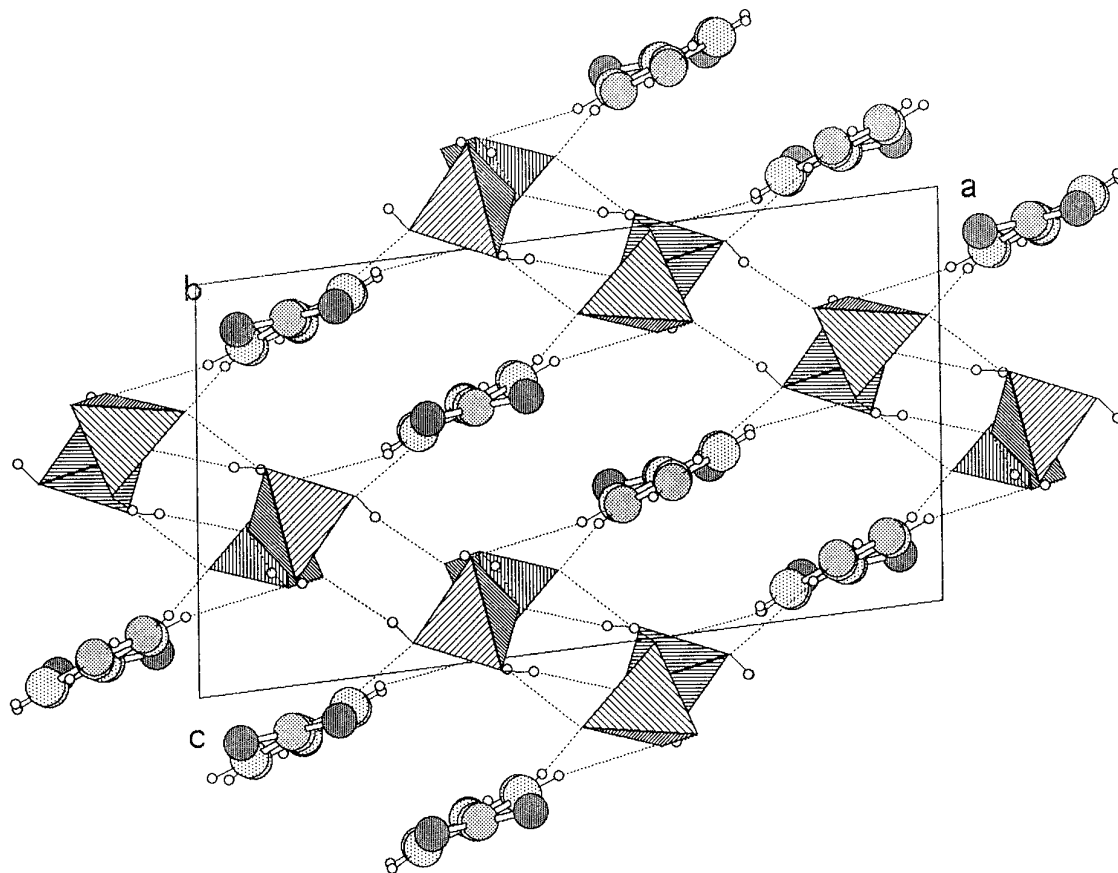

FIG. 2. Projection along **b** axis of the 2A5NPDPP structure evidencing the $(H_2PO_4^-, H_3PO_4)_n$ or $(H_5P_2O_8^-)_n$ layers separated by the 2A5NP$^+$ chains parallel to **b**. The broken lines represent hydrogen bonds. Small open circles, H atoms; dotted circles, C atoms; pale grey circles, N atoms; dark grey circles, O atoms.
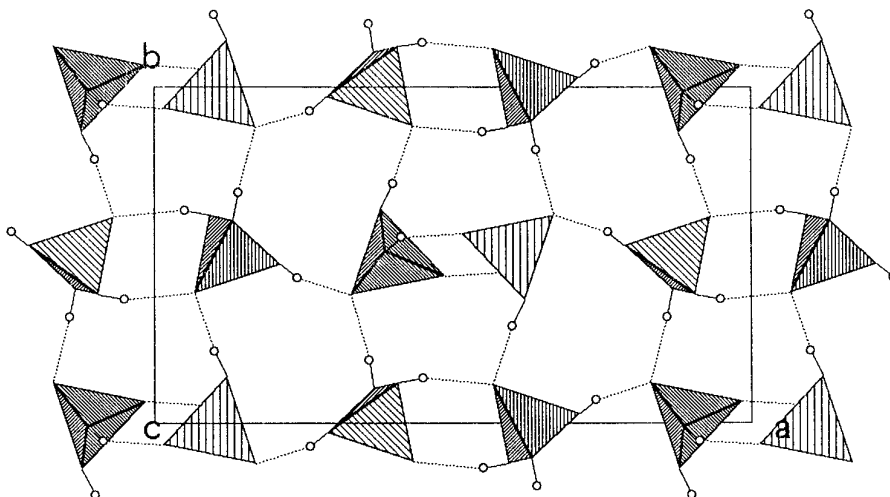
ZACCARO ET AL.

FIG. 3. Projection along **c** axis of the centrosymmetric $(H_5P_2O_8^-)_n$ layered polyanion in 2A5NPDPP.

for X-ray Crystallography (9). All calculations were carried out using the Enraf–Nonius SDP program (10) with a micro-Vax II computer. The structure was drawn using the MOLVIEW program (11).

Final atomic parameters are listed in Table 3. The main geometrical features of the PO_4^- tetrahedra and the 2-amino-5-nitropyridinium cation (2A5NP$^+$) are described in Table 4, the hydrogen bond scheme in Table 5. The values of the thermal anisotropic displacement parameters for nonhydrogen atoms and the list of ob-
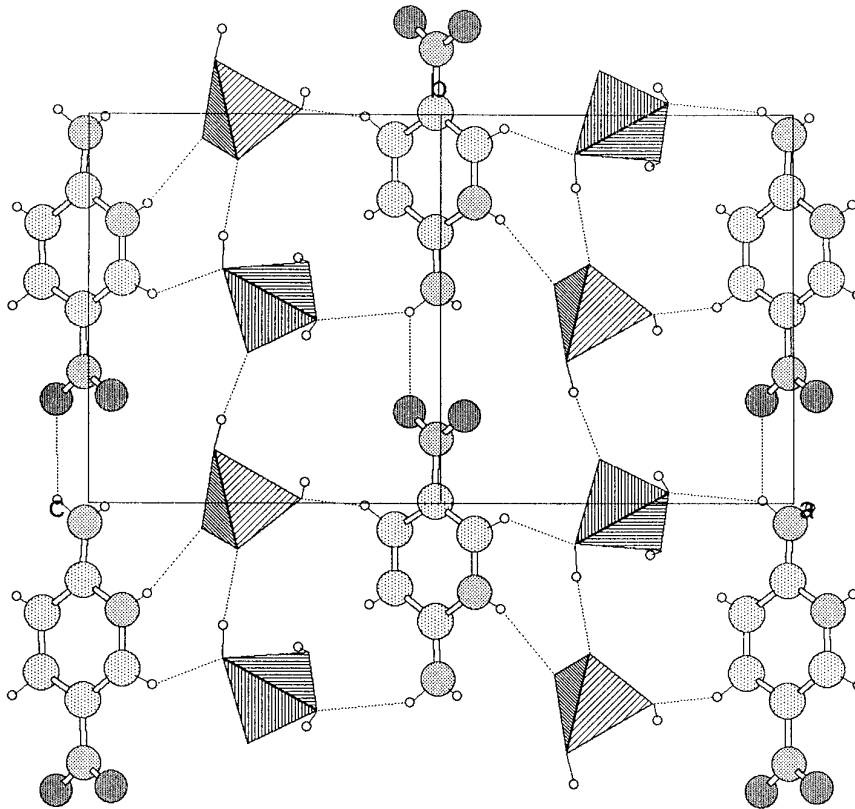

FIG. 4. A partial projection along the **(a + c)** direction of the 2A5NPDPP structure exhibiting the 2A5NP$^+$ infinite organic chains parallel to the inorganic layers and the related hydrogen bonds. Same legend as in Fig. 2.
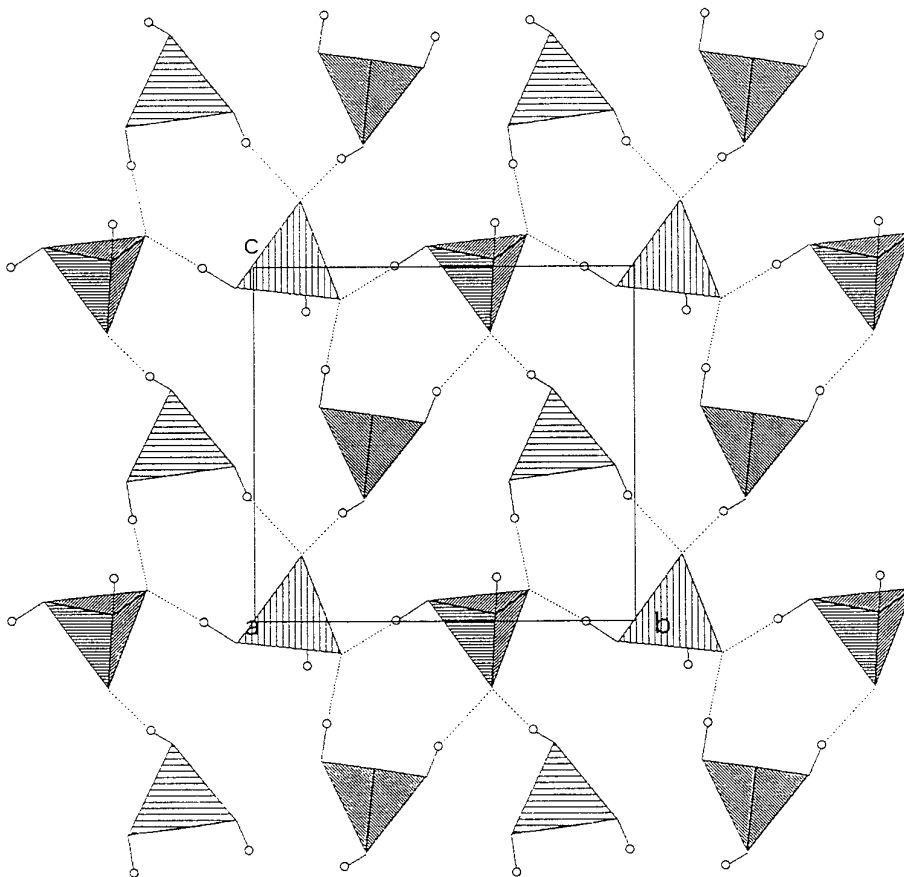
FIG. 5. A noncentrosymmetric $(H_5P_2O_8^-)_n$ layer of the anionic subnetwork in L-His. $+ \cdot H_2PO_4^- \cdot H_3PO_4$. One OH of the $H_2PO_4^-$ entity is linked to the cationic subnetwork.

served and calculated structure factors are available on request.

DISCUSSION

Figure 2 displays the crystal structure viewed along the **b** direction. The polyanion resulting from the aggregation of $H_2PO_4^-$ monomers and H_3PO_4 molecules through strong hydrogen bonds form inorganic layers parallel to the (**a + c, b**) plane (Figs. 2, 3). Infinite chains of 2A5NP$^+$ cations are anchored onto the anionic layers through weak hydrogen contacts (Fig. 4). The anionic subnetwork can be described as a centrosymmetric linkage of mixed entities [$H_2PO_4^-$, H_3PO_4] or as [$H_5P_2O_8^-$]. All H···O bonds which maintain the cohesion of this arrangement are characterized by relatively short distances, from 1.80 to 2.03(5) Å. Further, no oxygen atom belonging to the organic cation is involved in these hydrogen bonds. Such a subnetwork can be compared to those already observed in organic phosphate structures: the histidinium phosphate L-His. $+ \cdot H_2PO_4^- \cdot H_3PO_4$ (12) and the pyridinium phosphate $C_5H_6N^+ \cdot H_2PO_4^- \cdot H_3PO_4$ (13).

The former arrangement (Fig. 5) is two-dimensional and centrosymmetric, built from anionic chains $(H_2PO_4^-)_n$ (with a H···O bond distance of 1.54 Å between each unit) connected between them by H_3PO_4 molecules via H···O bonds from 1.68 to 1.87 Å. Nevertheless this hydrogen bonding network does not point out any direct bond between the acid molecules. Besides, this anionic layer is "open" in contrast to the one studied: an OH donor group of each $H_2PO_4^-$ unit connects the anionic subnetwork to the cationic one. The latter example is a two-dimensional arrangement of centrosymmetric aggregates $(H_2PO_4^-)_2$ interconnected by H_3PO_4 molecules (Fig. 6). As for the title compound, all the O–H···O bonds occur inside of the anionic subnetwork.

In these layered organizations of mixed phosphate entities, it is noteworthy that the O···O distances involved in hydrogen bonds (2.50 to 2.70 Å) are of the same order of magnitude as the O···O distances in $H_2PO_4^-$ or H_3PO_4 tetrahedra (2.41 to 2.56 Å); this should allow us to consider the $(H_5P_2O_8^-)_n$ subnetwork as a polyanion. The detailed geometry of $H_2PO_4^-$, H_3PO_4 entities shows that the P–O bonds are significantly shorter [1.503 to 1.522(3) Å] than
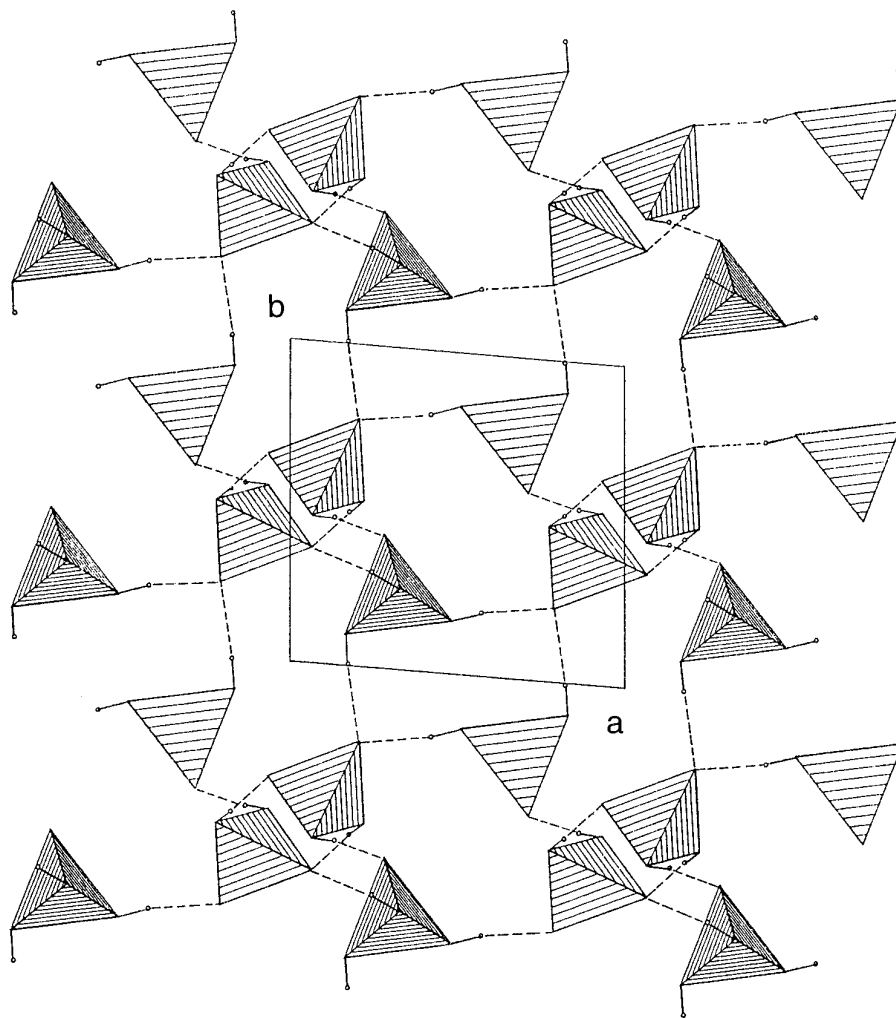
FIG. 6. The centrosymmetric anionic layer $(H_5P_2O_8^-)_n$ in pyridinium dihydrogenphosphate monophosphoric acid.

the P–OH bonds [1.543 to 1.557(3) Å] (Table 4), which is in accordance with the data relative to the protonated oxoanions (14).

With regards to the organic subnetwork, the 2A5NP$^+$ cations are linked by rather long (N)–H$\cdots$O bonds (2.33(6) Å) as to form chains running along the **b** direction. Each cation is anchored onto both adjacent anionic layers via multiple hydrogen bond N–H$\cdots$O and C–H$\cdots$O (Figs. 1, 3); that is to say, N2–H7$\cdots$O1 (2.39(6) Å) and C5–H11$\cdots$O5 (2.38(4) Å) on one side, N3–H8$\cdots$O7 (1.98(6) Å) and C2–H9$\cdots$O2 [2.55(5) Å] on the other side. The C–H$\cdots$O bonds have already been evidenced by several authors in molecular crystals (15–18). Moreover, when a large organic molecule becomes a cation, the charge is extended to the whole molecule and of course counterbalanced through all the H-donor groups. In this case the N–H$\cdots$O and C–H$\cdots$O contacts between the organic and inorganic subnetworks are of the same order of magni-

tude. In Table 5 have been listed all the D(donor)–H$\cdots$A (acceptor) hydrogen bonds with the outer limit of 2.55(5) Å for the H$\cdots$A distances (the sum of the van der Waals radii is $r_H + r_O = 1 + 1.54 = 2.54$ Å) and the inner limit of 130(5)° for the D–H$\cdots$A bond angles.

The geometrical features of the pyridinium ring are similar to those observed in other structures of 2-amino-5-nitropyridinium salts. The organic ring atoms are almost coplanar, the amino and nitro groups being exocyclic with large out-of-plane shifts (Table 4). The twist angle between the plane of the NO_2 group and the pyridinium ring is 15.2(3)°. Moreover, the C–NH_2 (1.319(6)Å) and C–NO_2 (1.445(5) Å) distances in the 2A5NP$^+$ cation are respectively shortened and lengthened with respect to the C–NH_2 (1.337(4) Å) and C–NO_2 (1.429(4) Å) observed in the 2-amino-5-nitropyridine molecular crystal (19). All the 2-amino-5-nitropyridinium cations hosted in various organic or inorganic matrices show the same changes in C–NH_2
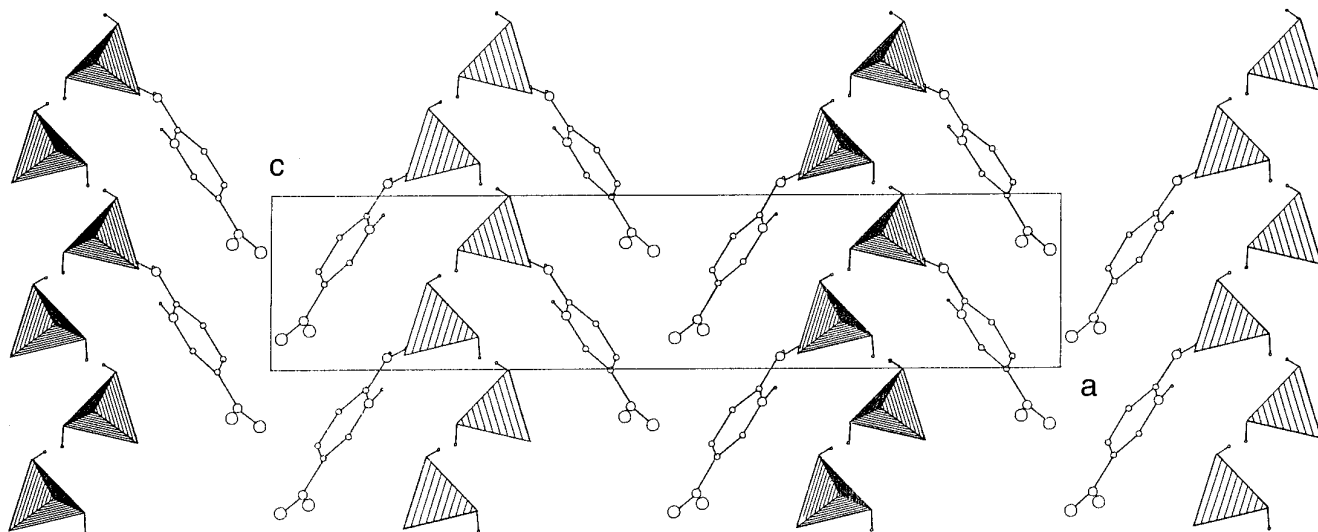
FIG. 7. The herringbone arrangement of chromophores in the 2A5NPDP structure.

and C–NO$_2$ distances, revealing a weak increase of π bond character in C–NH$_2$ and a decrease in C–NO$_2$. Indeed, the NH$^+$ group acts as a competitor electron acceptor group of NO$_2$, inducing changes (20) in molecular polarizability and color of crystals and solutions, in contrast to 2-amino-5-nitropyridine: all the crystals including the 2-amino-5-nitropyridinium cations display a shift of the absorption edge of 80 nm from 500 nm up to the blue region. $\lambda_{\text{cut-off}} = 500$ nm is the absorption limit for the 2-amino-5-nitropyridine or p-nitroaniline derivatives.
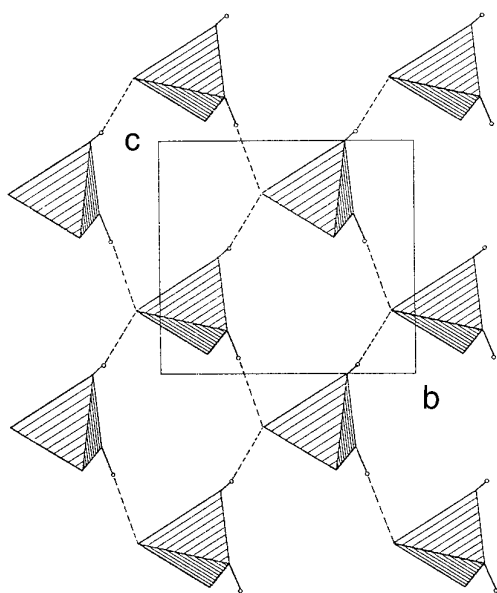
Now if the studied compound is compared to the noncentrosymmetric 2-amino-5-nitropyridinium dihydrogen phosphate (2A5NPDP) (2) (Fig. 7), the $(H_5P_2O_8^-)_n$ framework seems to be as cohesive as the $(H_2PO_4^-)_n$ framework of 2A5NPDP (Fig. 8), as emphasized by the values of hydrogen bonds in both anionic aggregates (Table 5). In 2A5NPDPP the unitary negative charge is distributed over all the $H_5P_2O_8^-$ entity: its volume is about twice that of $H_2PO_4^-$. The attraction between 2A5NP$^+$ cations and $(H_5P_2O_8^-)_n$ layers is thus weaker than that observed between 2A5NP$^+$ cations and $(H_2PO_4^-)_n$ layers: this situation is clearly evidenced by comparison of the N–H$\cdots$O contacts in both structures (Table 5). So the capture of the H$_3$PO$_4$ solvent molecules by the $(H_2PO_4^-)_n$ layered aggregates results in a charge dilution with the formation of a new $(H_5P_2O_8^-)_n$ polyaggregate and in decay of cation–anion cohesion with respect to that observed in the 2A5NPDP herringbone framework. In fact, herringbone structures containing 2A5NP$^+$ cations are built through short NH$\cdots$O or N–H$\cdots$Cl(Br) bonds (21): these strong cation–anion attractions prevail over multiple weak interactions between cations as C–H$\cdots$O and π–π bonds favorable to an opposite arrangement of them, i.e., to the local centrosymmetry.

CONCLUSION

An empirical rule directing the formation of herringbone motifs of 2-amino-5-nitropyridinium cations has been established from several crystal structure investigations: chained or layered anionic aggregates favor herringbone subnetworks, always resulting in noncentrosymmetric structures (4, 5). The 2A5NPDPP crystal structure shows the role played by the volume to charge ratio of the mono-

FIG. 8. The noncentrosymmetric anionic subnetwork $(H_2PO_4^-)_n$ in 2A5NPDP.

mer $H_5P_2O_8^-$: the too low charge of the host anionic aggregate $(H_5P_2O_8^-)_n$, compared to that of $(H_2PO_4^-)_n$, weakens the cation–anion cohesion, ruining the eventual anchorage of chromophores onto anions through three short hydrogen bonds able to induce a noncentrosymmetric herringbone structure.

REFERENCES

1. R. Masse, M. Bagieu-Beucher, J. Pécaut, J. P. Levy, and J. Zyss, *Nonlinear Opt.* **5,** 413 (1993).
2. R. Masse and J. Zyss, *J. Mol. Eng.* **1,** 141 (1991).
3. J. Pécaut, J. P. Levy, and R. Masse, *J. Mater. Chem.* **3**(10), 999 (1993).
4. J. Pécaut and R. Masse, *J. Mater. Chem.* **4**(12), 1851 (1994).
5. Y. Le Fur, M. Bagieu-Beucher, R. Masse, J. F. Nicoud and J. P. Levy, *Chem. Mater.* **8**(1), 68 (1996).
6. M. Bagieu-Beucher, R. Masse, and D. Tran Qui, *Z. Anorg. Allg. Chem.* **5,** 606 (1991).
7. K. L. Elmore, J. D. Hatfield, R. L. Dunn, and A. D. Jones, *J. Phys. Chem.* **69**(10), 3520 (1965).
8. P. Main, L. Lessinger, M. M. Woolfson, G. Germain, and J. P. Declercq, "MULTAN77. A System of Computer Programs for the Automatic Solution of Crystal Structures from X-ray Diffraction Data." Universities of York and Louvain, 1977.
9. "International Tables for X-ray Crystallography," Vol. IV, Table 2-2B. Kynoch Press, Birmingham.
10. "Structure Determination Package RSX11M." Enraf-Nonius, Delft, The Netherlands, 1979.
11. J. M. Cense, *Tetrahedron Comput. Methods* **2,** 65 (1989).
12. R. H. Blessing, *Acta Crystallogr. Sect. B* **42,** 613 (1986).
13. R. Masse and I. Tordjman, *Acta Crystallogr. Sect. C* **46,** 606 (1990).
14. G. Ferraris and G. Ivaldi, *Acta Crystallogr. Sect. B* **40,** 1 (1984).
15. O. Kennard and R. Taylor, *J. Am. Chem. Soc.* **104,** 5063 (1982).
16. G. R. Desiraju, *Acc. Chem. Res.* **24,** 290 (1991).
17. T. Steiner and W. Saenger, *J. Am. Chem. Soc.* **115,** 4540 (1993).
18. T. Steiner and W. Saenger, *Acta Crystallogr. Sect. B* **50,** 348 (1994).
19. C. B. Aakeröy and M. Nieuwenhuyzen, to be published.
20. M. Dewar, *J. Chem. Soc.,* 2329 (1950).
21. R. Masse, *Nonlinear Opt.* **9,** 113 (1995).